THE JOURNAL OF PHYSICAL CHEMISTRY LETTERS
A JOURNAL OF THE AMERICAN CHEMICAL SOCIETY

pubs.acs.org/JPCL

Letter

# Following Metal-to-Ligand Charge-Transfer Dynamics with Ligand and Spin Specificity Using Femtosecond Resonant Inelastic X-ray Scattering at the Nitrogen K-Edge

Raphael M. Jay, Sebastian Eckert, Benjamin E. Van Kuiken,* Miguel Ochmann, Markus Hantschmann, Amy A. Cordones, Hana Cho, Kiryong Hong, Rory Ma, Jae Hyuk Lee, Georgi L. Dakovski, Joshua J. Turner, Michael P. Minitti, Wilson Quevedo, Annette Pietzsch, Martin Beye, Tae Kyu Kim, Robert W. Schoenlein, Philippe Wernet, Alexander Föhlisch, and Nils Huse*

Cite This: *J. Phys. Chem. Lett.* 2021, 12, 6676−6683

Read Online

ACCESS | Metrics & More | Article Recommendations | Supporting Information

**ABSTRACT:** We demonstrate for the case of photoexcited $[Ru(2,2'\text{-bipyridine})_3]^{2+}$ how femtosecond resonant inelastic X-ray scattering (RIXS) at the ligand K-edge allows one to uniquely probe changes in the valence electronic structure following a metal-to-ligand charge-transfer (MLCT) excitation. Metal−ligand hybridization is probed by nitrogen-1s resonances providing information on both the electron-accepting ligand in the MLCT state and the hole density of the metal center. By comparing to spectrum calculations based on density functional theory, we are able to distinguish the electronic structure of the electron-accepting ligand and the other ligands and determine a temporal upper limit of (250 ± 40) fs for electron localization following the charge-transfer excitation. The spin of the localized electron is deduced from the selection rules of the RIXS process establishing new experimental capabilities for probing transient charge and spin densities.

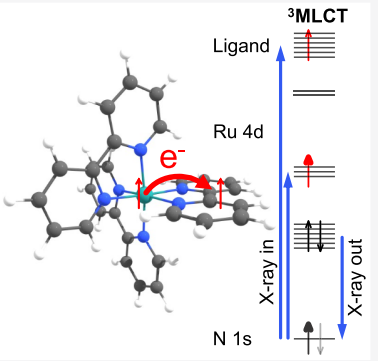


Charge-transfer excitations are the initiating step of many photochemical reactions involving transition metal complexes. Owing to its wide applicability in fields like light-harvesting[1,2] and photocatalysis,[3] the metal-to-ligand charge-transfer (MLCT) excitation in $[Ru(bpy)_3]^{2+}$ (where bpy = 2,2′-bipyridine) constitutes the prototypical example of such a process. Specifically, the system and its derivatives are investigated as photoinduced electron donors in potential inflammatory sensors,[4] water splitting,[5] and enzyme triggering reactions[6] and as dye sensitizer models[7−10] as well as active moieties in phototherapy[11,12] and molecular switches.[13,14] On an intramolecular level, the charge-transfer process is initiated by an optical excitation, which elevates a Ru-4d electron into an unoccupied bpy $\pi^*$ orbital. This effectively oxidizes the metal center, while reducing one bpy ligand and thereby breaking the symmetry of the electronic ground state. Ultrafast transient absorption and emission studies have established that the lowest charge-transfer excitation of many polypyridyl iron(II) and ruthenium(II) complexes from their singlet ground-state results in the initial population of a $^1$MLCT state, which has a substantial spin admixture of the lower-lying $^3$MLCT manifold, resulting in very fast intersystem crossing into a $^3$MLCT state within tens of femtoseconds.[15−17] In $[Ru(bpy)_3]^{2+}$, the possibly delocalized initial charge distribution of the MLCT state triggers a solvent response that stabilizes the charge distribution of the MLCT state. From optical spectroscopy, it has been concluded that the transferred electron is localized on one of the three bpy ligands.[18−20] The localized electron will still hop between ligands but is stabilized by solute−solvent interactions analogous to a polaron in a crystalline solid (an excited electron localized in the center of a lattice distortion that forms in response to the sudden creation of a mobile charge carrier). While optical spectroscopy provides robust measures of the involved time scales, the broad and overlapping spectral features are often difficult to relate to the electronic structure and spin configuration of the excited state.[13,21−24] Ideally, spectroscopic information from specific atomic sites would allow following and characterizing the relaxation from the initially excited charge-transfer excitation to localized partial charge densities, i.e., an electron−hole pair determined by Coulomb and covalent metal−ligand interactions.

Atomic site-sensitivity can be provided by X-ray spectroscopy. By projecting a highly localized core orbital onto

**Received:** April 30, 2021
**Accepted:** June 4, 2021
**Published:** July 14, 2021

delocalized valence orbitals in an X-ray absorption process, the chemical environment around the absorbing atomic species can be characterized. Picosecond X-ray absorption experiments at the Ru K- and L-edge of $[Ru(bpy)_3]^{2+}$ and similar systems established subtle changes in metal−ligand bond lengths as a result of the formation of the $^3$MLCT state.[25,26] More importantly, changes in the local valence electronic structure and the ligand field around the Ru center, which result from the metal-center's photoinduced oxidation, could be determined using L-edge absorption spectroscopy.[8,25] However, with the underlying metal 2p → 4d transitions primarily being sensitive to the hole in the metal d orbitals, L-edge absorption spectroscopy is limited in providing information on the transferred electron. The latter is only indirectly observed through changes in covalent metal−ligand interactions which modulate the Coulomb and exchange interactions that influence the L-edge line shape. An ultrafast spectroscopic probe that can adapt both a metal- and ligand-centered view, within one process, would indeed provide the necessary information on the transient charge density of an intramolecular electron−hole pair.

We present femtosecond resonant inelastic soft X-ray scattering[27] (RIXS) at the K-edge of ligand atoms, specifically at the nitrogen K-edge,[28−32] as such a probe: Resonant N 1s core-excitations, which promote ligand core−electrons to unoccupied metal-centered orbitals with subsequent resonant emission from ligand-centered valence electrons, report on the charge density of the ligand modulated by charge density changes at the metal. This provides simultaneous information on the transferred electron as well as the hole on the metal and is manifested in valence excitation spectra deep into the vacuum ultraviolet regime specific to certain chemical sites.[33,34] Due to the underlying spin selection rules governing the dipole transitions of the RIXS process in the soft X-ray photon range, the contained spectral information also gives information on different spin states, since specific valence excited final states are only dipole-allowed in specific spin configurations of the system.

Thus far, time-resolved RIXS in the soft X-ray regime has been employed in L-edge measurements on iron complexes in order to follow the evolution of the valence electronic structure locally at the metal center during ligand-exchange[35−37] and charge-transfer dynamics.[38,39] At the N K-edge, however, only time-resolved X-ray absorption studies on transition metal complexes have previously been realized,[32,40,41] while time-resolved RIXS has only been used to study the transiently deprotonated N site in an organic molecule.[34] In the case of charge-transfer excited $[Ru(bpy)_3]^{2+}$, time-resolved N K-edge RIXS allows one to directly access, distinguish, and evaluate the valence electronic structure of the different bpy groups (electron-accepting and non-electron-accepting) and follow the electron−hole pair in time since the spectroscopic probe also includes the metal valence charge density. Thereby, our results and analysis provide a robust temporal upper limit for electron and hole localization by exploiting the sensitivity of our experimental method to the dynamics of charge-transfer excitations for both electron and hole. We utilize the spin-selection rules of N K-edge RIXS to demonstrate how such ultrafast measurements can follow the spin crossover associated with the MLCT excitation.

Figure 1 shows the molecular structure as well as steady-state RIXS data of $[Ru(bpy)_3]^{2+}$ measured at the N K-edge. The data is acquired by simultaneously scanning the incident

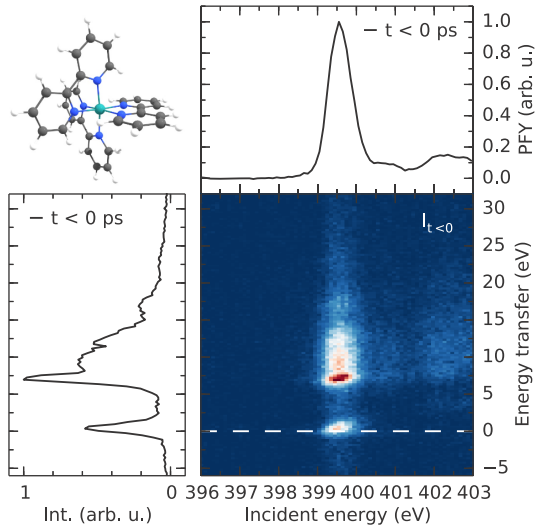


**Figure 1.** DFT-optimized molecular structure and steady-state N K-edge RIXS map of aqueous $[Ru(bpy)_3]^{2+}$. By integrating along the energy transfer axis, the PFY spectrum (shown on top) is acquired. On the left, a resonant emission spectrum is displayed, which is acquired by integrating across the main absorption line.

energy and pump−probe delay. By integration over all pump−probe delays $t < 0$, the steady-state RIXS map is generated. The RIXS map is displayed as a function of the energy transfer, which corresponds to the energy of the valence-excited final states of the RIXS process. By integration along the energy transfer axis, the partial fluorescence yield (PFY) X-ray absorption spectrum (XAS) can be generated. It is dominated by a single intense transition at 399.6 eV, which can be assigned to the elevation of a N 1s core−electron into the unoccupied bpy $\pi^*$ manifold. In the two-step approximation of the RIXS process, the core-excitation is followed by a resonant emission step, whose spectrum is additionally shown on the left in Figure 1. It is acquired by integrating the RIXS map along the incident energy axis across the main absorption resonance between 399.15 and 399.85 eV. The resonant emission spectrum exhibits a feature at 0 eV energy transfer corresponding to elastic scattering. The most intense feature is located at 7 eV energy transfer followed by additional features with lower intensity up until 25 eV energy transfer. The general shape of the spectrum is similar to previous measurements on $[Fe(bpy)_3]^{2+}$, where the resonant emission originated mostly from the recombination of electrons occupying ligand-centered orbitals of the bpy ligand with the N 1s core-hole.[28]

Figure 2a shows the PFY XAS spectrum of $[Ru(bpy)_3]^{2+}$ for positive and negative pump−probe delays. The individual spectra are normalized to the number of FEL shots, which are included in the respective delay range. The spectra are then scaled so that the maximum of the ground state spectrum is unity to visualize the relative magnitude of the spectral changes upon laser excitation. The absorption of an optical photon causes a decrease of the main X-ray absorption resonance as well as an intensity increase before and after the main resonance. To isolate the laser-induced changes in the PFY spectrum, Figure 2b shows the difference between the two spectra from Figure 2a. The observed spectral changes upon photoexcitation are well described by the calculated difference spectrum. The calculation is based on time-dependent density functional theory (TD-DFT) and carried out for each unique N atom. In the case of the ground state, the molecule is


https://doi.org/10.1021/acs.jpclett.1c01401
J. Phys. Chem. Lett. 2021, 12, 6676−6683

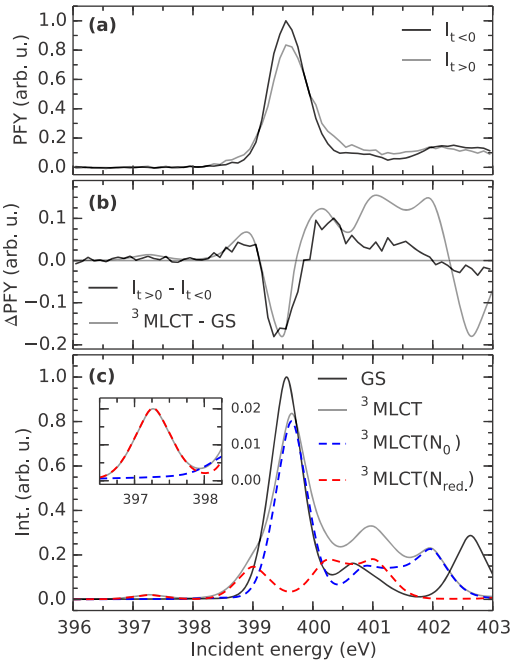


**Figure 2.** (a) PFY XAS of $[Ru(bpy)_3]^{2+}$ for negative and positive pump−probe delays in the range of −1.5 to +1.5 ps. (b) Difference PFY between the two spectra from part a compared to a calculated difference spectrum between the $^3$MLCT state and the ground state of $[Ru(bpy)_3]^{2+}$. (c) Calculated spectra of the ground state (GS) and the $^3$MLCT. The spectrum of the $^3$MLCT state is further broken down into contributions from the two $N_{red.}$ atoms of the electron-accepting bpy ligand and the four $N_0$ sites of the spectator ligands.

sufficiently symmetric that the XAS spectrum resulting from creation of a core-hole on any one of the N atoms is equivalent. Due to the symmetry reduction associated with the MLCT excitation, however, the spectrum of the $^3$MLCT is the sum of six TD-DFT spectra. The calculated difference spectrum is then generated as the weighted difference between the excited and ground state spectrum and scaled to the maximum of the depletion in the experimental data at 399.45 eV. The calculation shows very good agreement with the experiment, reproducing the depletion of the main absorption line at 399.45 eV and the signal increase below and above the main absorption line.

In order to rationalize the dominant core-excitations causing the spectral trends observed in the experimental PFY spectrum, Figure 2c shows the simulated spectra of the ground state and the $^3$MLCT state as well as a breakdown of the $^3$MLCT spectrum into contributions from different ligands. The spectrum of the $^3$MLCT can be divided into contributions from the electron-accepting reduced bpy group (denoted as $N_{red.}$) and the two other bpy groups (denoted as $N_0$), which merely act as spectators of the charge-transfer excitation. This distinction is motivated by the observation that the orbital of the transferred electron is clearly localized at a single bpy group (see Supporting Information). The good agreement of such a description with experiment reinforces previous notions of a localized electron in the $^3$MLCT state[19] and, for the first time, ties the associated reduction of symmetry to differences in the underlying electronic structure between the two types of ligands.

The general character of the spectrum of the $N_0$ sites is very similar to the ground state spectrum, however slightly shifted to higher energies. This is due to the $N_0$ sites mainly experiencing the effective oxidation of the Ru center as a result of the charge-transfer excitation. The depopulation of the Ru $t_{2g}$ orbitals reduces the Coulomb-repulsion between the $N_0$ ligands and the metal. This leads to an increase in $\sigma$-donation, a relation, which has previously been observed also for other charge-transfer excitations.[39,42] These changes in covalency cause the N 1s core-level energies to drop by on average 0.4 eV at the $N_0$ sites, which shifts the transitions to higher energy.[32,43]

A completely different spectral behavior can be observed for the $N_{red.}$ sites. There, the intensity of the main $\pi^*$ resonance is drastically reduced and shifted to lower energy (see Supporting Information for associated difference density) causing the emergence of the pre-edge feature at 398.8 eV in the experimental difference spectrum in Figure 2b. The energetic shift can be associated with the increase of electron density on the ligand caused by the MLCT process and results in a 0.5 eV increase in the N 1s orbital energy. The decrease in intensity can be attributed to the fact that the lowest-lying $\pi^*$ orbital is half-filled in the MLCT state. Additionally, the calculations in Figure 2c suggest a new low-energy resonance to appear for the $N_{red.}$ sites at 397.3 eV. The character of this resonance can be clearly assigned to a N 1s → Ru $t_{2g}$ excitation (see Supporting Information). This feature becomes visible in the $N_{red.}$

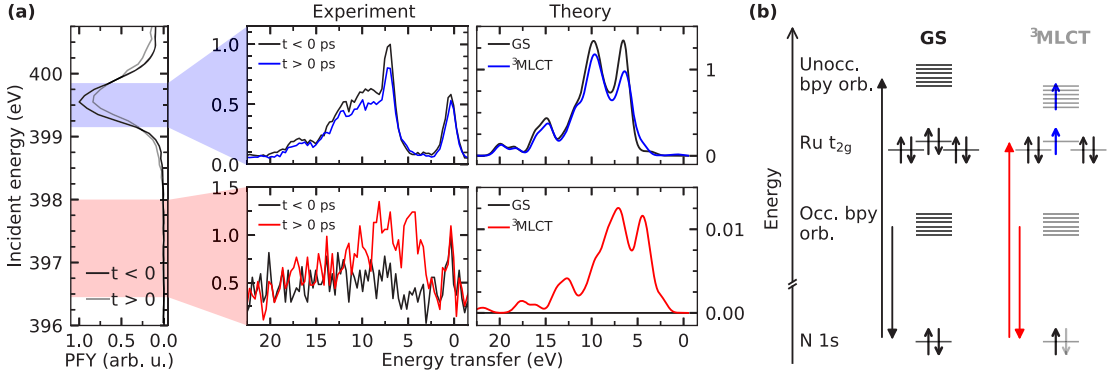


**Figure 3.** (a) Experimental RIXS spectra for negative and positive pump−probe delays compared to calculated RIXS spectra. The experimental spectra are acquired by integrating the incident energy across the regions marked in the PFY spectrum displayed on the left. The calculated spectra are based on the single-electron approximation and evaluated for excitation energies within the experimental incident energy regions. (b) Schematic representation of the observed RIXS transitions based on a single-electron picture.



https://doi.org/10.1021/acs.jpclett.1c01401
J. Phys. Chem. Lett. 2021, 12, 6676−6683

spectrum because the increase in the $N_{red.}$ 1s orbital energy and the presence of the $t_{2g}$ hole yield a lowered excitation energy, which is separated from the rest of the N K-edge XAS spectrum. Second, while the N 1s → Ru $t_{2g}$ transition is formally forbidden, the Ru-based $t_{2g}$ acceptor orbital exhibits a small amount (~2%) of $N_{red.}$ p-character providing dipole intensity. The new transition therefore constitutes a direct fingerprint for the depopulation of metal d orbitals and thus local oxidation of the metal center by the MLCT excitation as seen from the N K-edge.[41] It should be noted that the experimental difference PFY spectrum shows no significant intensity increase in the range of 397.3 eV. However, in the following, we provide unambiguous experimental evidence for the presence of this transition, which allows one to selectively access the reduced bpy ligand of the $^3$MLCT state and extract the corresponding site-specific RIXS spectrum.

Figure 3a shows experimental RIXS spectra integrated over the incident energy region of the ground state $\pi^*$ resonance (marked blue) as well as the $t_{2g}$ resonance (marked red) for positive and negative pump−probe delays. Most importantly, the latter shows an emergence of intensity at energy transfers between 3 and 13 eV following the optical excitation. The detected fluorescence in this range clearly demonstrates the presence of a resonant excitation for the $^3$MLCT state at this incident energy as predicted by the calculations in Figure 2c. This is despite the resonance not rising above the noise level in the experimental PFY difference spectrum in Figure 2b, because it is acquired by integrating over a wide range of energy transfers. In the RIXS spectrum recorded at the ground state $\pi^*$ resonance, a uniform decrease of intensity up until 20 eV energy transfer can be observed reflecting the overall decrease of the main absorption line in the PFY spectrum upon optical excitation.

In order to rationalize the spectral features in the transient RIXS spectra, calculated RIXS spectra based on a one-electron picture (see Supporting Information) are additionally presented in Figure 3a. The calculated RIXS spectra show good qualitative agreement with the experiment. The overall decrease in intensity at the ground state $\pi^*$ resonance is reproduced as well as the emergence of fluorescence in the range of the $t_{2g}$ resonance which is absent before the optical excitation. It should be emphasized that, despite minor variations, the general shape of the RIXS spectra is maintained after the optical excitation and is very similar at the two different excitation energies. This indicates that the orbitals and their energies involved in the X-ray emission step of the RIXS process largely remain the same and the variations in final state energies can for the most part be rationalized by the underlying differences in X-ray excitation energies in the different incident energy regions. This is illustrated by the molecular orbital diagram displayed in Figure 3b. As has been mentioned previously, the ground state RIXS spectrum following an excitation at the $\pi^*$ resonance is characterized by electronic decays dominantly from occupied bpy orbitals resulting in ligand-centered valence-excited final states.[28] In the case of at the newly opened $t_{2g}$ resonance, however, the system is core-excited at lower incident energy. With emission energies remaining constant, this creates new low-energy valence excited final states of dominantly ligand-to-metal charge-transfer (LMCT) character.

Additionally, due the half-filled Ru $t_{2g}$ level in the $^3$MLCT state (compare Figure 3b), core-excitation at the $t_{2g}$ resonance creates exclusively spin-down core-holes. The Pauli exclusion principle for Fermions and spin selection rules of dipole transitions ($\Delta S = 0$) therefore dictate that only spin-down electrons can subsequently fill the N 1s core-hole following the core-excitation. This allows one to retrieve information about the spin state of the system from the spectra measured at the $t_{2g}$ resonance, since the spin-up electron occupying the bpy $\pi^*$ orbital in the $^3$MLCT state cannot recombine with the spin-down N 1s core-hole, although the two orbitals have significant overlap. Such a transition is, however, allowed as long as the system is in the initially populated $^1$MLCT configuration. Exploiting these selection rules therefore introduces sensitivity to the spin state of the charge-transfer excited state. As will be shown in the following, this opens up novel opportunities to temporally follow the earliest transients involved in the charge-transfer dynamics.

The spectral changes discussed so far were averaged over all negative and positive delays and have been assigned to dominantly correspond to the presence of the ground and the $^3$MLCT state, respectively. To follow the spectral changes as a function of pump−probe delay, Figure 4 shows the full

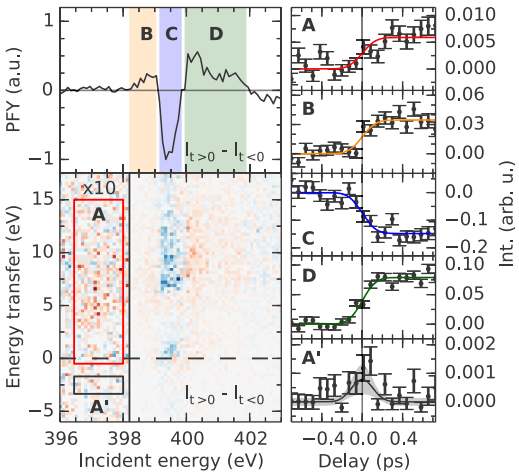


**Figure 4.** Delay traces acquired by integration over spectral ranges in the difference PFY spectrum as well as the difference RIXS map. The temporal evolution of the spectral signatures can for the most part be described by the emergence of the $^3$MLCT state within the time-resolution of the experiment.

difference RIXS map with the experimental PFY difference spectrum from Figure 2b above. Incident energy regions A and C correspond to the regions discussed in Figure 3, while B and D cover regions before and after the main edge. To increase the signal-to-noise ratio, region A is restricted to the area for which an increase in intensity could be observed in Figure 3 (elastic scattering as well as positive energy losses). Area A′ is additionally introduced as a spectral region which will be discussed separately. By integrating the scattered photons within the marked regions for time intervals of 70 fs, the time traces shown on the right of Figure 4 can be extracted (error-bars deduced from $\sqrt{N}$ of detected photons within a spectral region). To visualize the relative magnitude of the spectral changes in the individual regions, the traces are normalized to the integrated signal of region C before time-zero (intensity of the ground state $\pi^*$-resonance). The relative changes detected in regions A to D are modeled by a step-function convolved with a Gaussian. The good description of the data by the fit demonstrates that the dominant signal changes happen


https://doi.org/10.1021/acs.jpclett.1c01401
J. Phys. Chem. Lett. 2021, 12, 6676−6683

synchronously and within the (250 ± 40) fs rise-time of the Gaussian-broadened step-function. This assessment again confirms the previously drawn conclusion that the $^3$MLCT state is the species dominantly contributing to the observed spectral changes. Furthermore, due to the good description of the observed spectral changes by a localized $^3$MLCT state, the retrieved rise-time of 250 fs can be established as an upper limit for electron localization in $[Ru(bpy)_3]^{2+}$ in agreement with previous transient absorption experiments.[19,20]

Traces of an additional species can be identified which do not correspond to the formation of the $^3$MLCT state, but instead point toward the short-lived $^1$MLCT state. For a discussion of this observation, we turn to region A′, which is located at the $t_{2g}$ resonance of the $^3$MLCT state and at negative energy transfer (compare Figure 4). As discussed previously, the core-excitation at the $t_{2g}$ resonance only creates spin-down nitrogen-1s core-holes. Due to spin selection rules, this core-hole can therefore only be efficiently filled by the decay of the transferred electron via a dipole transition as long as the system is in the initial $^1$MLCT state with a singlet spin configuration right after the optical excitation. Region A′ is thus centered at a negative energy transfer which exactly corresponds to the energy of the optical excitation (see Experimental Details). Conceptually, this can be understood as energy, which is deposited in the system by absorption of an optical photon and subsequently added to the energy of the core-excitation. An anti-Stokes transition[37] then results in a net gain in energy of the emitted X-rays and the final state character of this transition therefore corresponds to the singlet ground state of $[Ru(bpy)_3]^{2+}$. Such anti-Stokes transitions have been previously observed in L-edge RIXS measurements[35−37] and calculations,[38] where they have been characterized to constitute unique spectroscopic fingerprints of short-lived transient intermediates during photochemical reactions. The delay trace derived from region A′, however, cannot be considered statistically significant evidence for an anti-Stokes line. This is not surprising given that the lifetime of the $^1$MLCT state has been reported to be on the order of 20 fs by theory[44] as well as experiment.[16] Still, the increase in intensity around time-zero points toward the presence of such a feature. To guide the eye, the delay trace retrieved from region A′, is therefore fitted with a Gaussian function (shaded area refers to 95% confidence interval), whose temporal width corresponds to the previously determined signal rise-time and exceeds the $^1$MLCT lifetime by 1 order of magnitude. While the data presented here does not constitute an unambiguous detection of the $^1$MLCT state, it provides a template for the design of future experiments with the improved time-resolution and count rates at upcoming high-repetition rate XFEL facilities.

In summary, we have shown how time-resolved RIXS at the ligand K-edge can be a powerful tool to follow charge-transfer dynamics in transition metal complexes. In particular, by directly evaluating the differences in the electronic structure between the electron-accepting and nonelectron-accepting ligands, the method confirms the localized nature of the $^3$MLCT state of $[Ru(bpy)_3]^{2+}$ on time-scales upward of 250 fs and uniquely provides valence excitation spectra specific to the reduced ligand. Furthermore, by exploiting the stringent selection rules of the RIXS process, new experimental schemes could be proposed which would allow one to capture and characterize the elusive primary $^1$MLCT state. Such experiments, which are expected to be routinely performed at upcoming high-repetition rate X-ray free electron lasers, would nicely complement studies using femtosecond K$\beta$ X-ray emission spectroscopy, a technique that is powerful in terms of determining the spin-state of the metal center but, due to its purely metal-centric character, struggles to distinguish between $^1$MLCT and $^3$MLCT states.[45−48]

## ■ ASSOCIATED CONTENT

### Supporting Information

The Supporting Information is available free of charge at https://pubs.acs.org/doi/10.1021/acs.jpclett.1c01401.

Chemicals and materials and experimental and computation details and figured showing isosurfaces of selected molecular orbitals (Figure S1), transition orbitals (Figure S2), and additional RIXS data (Figures S3) not shown in the main text (PDF)

## ■ AUTHOR INFORMATION


### Corresponding Authors

**Benjamin E. Van Kuiken** − *European XFEL, 22869 Schenefeld, Germany;* orcid.org/0000-0002-3650-7765; Email: benjamin.van.kuiken@xfel.eu

**Nils Huse** − *Department of Physics, University of Hamburg and Center for Free-Electron Laser Science, 22761 Hamburg, Germany;* orcid.org/0000-0002-3281-7600; Email: nils.huse@uni-hamburg.de

### Authors

**Raphael M. Jay** − *Institut für Physik und Astronomie, Universität Potsdam, 14476 Potsdam, Germany;* Present Address: Department of Physics and Astronomy, Uppsala University, 75120 Uppsala, Sweden; orcid.org/0000-0001-9607-8264

**Sebastian Eckert** − *Institut für Physik und Astronomie, Universität Potsdam, 14476 Potsdam, Germany; Institute for Methods and Instrumentation for Synchrotron Radiation Research, Helmholtz-Zentrum Berlin für Materialien und Energie, 12489 Berlin, Germany;* orcid.org/0000-0002-1310-0735

**Miguel Ochmann** − *Department of Physics, University of Hamburg and Center for Free-Electron Laser Science, 22761 Hamburg, Germany*

**Markus Hantschmann** − *Institut für Physik und Astronomie, Universität Potsdam, 14476 Potsdam, Germany; Institute for Methods and Instrumentation for Synchrotron Radiation Research, Helmholtz-Zentrum Berlin für Materialien und Energie, 12489 Berlin, Germany*

**Amy A. Cordones** − *Ultrafast X-ray Science Lab, Chemical Sciences Division, Lawrence Berkeley National Laboratory, Berkeley, California 94720, United States;* Present Address: Stanford PULSE Institute, SLAC National Accelerator Laboratory, Menlo Park, California 94025, United States; orcid.org/0000-0001-9897-5380

**Hana Cho** − *Ultrafast X-ray Science Lab, Chemical Sciences Division, Lawrence Berkeley National Laboratory, Berkeley, California 94720, United States; Department of Chemistry and Chemistry Institute of Functional Materials, Pusan National University, Busan 46241, South Korea;* Present Address: Inorganic Metrology Group, Division of Chemical and Biological Metrology, Korea Research Institute of Standards and Science, Daejeon 34113, Republic of Korea; orcid.org/0000-0001-8367-3259




https://doi.org/10.1021/acs.jpclett.1c01401
J. Phys. Chem. Lett. 2021, 12, 6676−6683

**Kiryong Hong** − *Department of Chemistry and Chemistry Institute of Functional Materials, Pusan National University, Busan 46241, South Korea;* Present Address: Gas Metrology Group, Division of Chemical and Biological Metrology, Korea Research Institute of Standards and Science, Daejeon 34113, Republic of Korea; orcid.org/0000-0002-3590-3635

**Rory Ma** − *Department of Physics, University of Hamburg and Center for Free-Electron Laser Science, 22761 Hamburg, Germany; Department of Chemistry and Chemistry Institute of Functional Materials, Pusan National University, Busan 46241, South Korea;* Present Address: Pohang Accelerator Laboratory, Pohang, Gyeongbuk 37673, Republic of Korea

**Jae Hyuk Lee** − *Ultrafast X-ray Science Lab, Chemical Sciences Division, Lawrence Berkeley National Laboratory, Berkeley, California 94720, United States;* Present Address: Pohang Accelerator Laboratory, Pohang, Gyeongbuk 37673, Republic of Korea

**Georgi L. Dakovski** − *Linac Coherent Light Source, SLAC National Accelerator Laboratory, Menlo Park, California 94025, United States*

**Joshua J. Turner** − *Linac Coherent Light Source, SLAC National Accelerator Laboratory, Menlo Park, California 94025, United States; Stanford Institute for Materials and Energy Sciences, Stanford University, Stanford, California 94305, United States*

**Michael P. Minitti** − *Linac Coherent Light Source, SLAC National Accelerator Laboratory, Menlo Park, California 94025, United States*

**Wilson Quevedo** − *Institute for Methods and Instrumentation for Synchrotron Radiation Research, Helmholtz-Zentrum Berlin für Materialien und Energie, 12489 Berlin, Germany*

**Annette Pietzsch** − *Institute for Methods and Instrumentation for Synchrotron Radiation Research, Helmholtz-Zentrum Berlin für Materialien und Energie, 12489 Berlin, Germany*

**Martin Beye** − *Institute for Methods and Instrumentation for Synchrotron Radiation Research, Helmholtz-Zentrum Berlin für Materialien und Energie, 12489 Berlin, Germany;* Present Address: Deutsches Elektronen-Synchrotron DESY, 22607 Hamburg; orcid.org/0000-0002-3924-2993

**Tae Kyu Kim** − *Department of Chemistry, Yonsei University, Seoul 03722, Republic of Korea;* orcid.org/0000-0002-9578-5722

**Robert W. Schoenlein** − *Ultrafast X-ray Science Lab, Chemical Sciences Division, Lawrence Berkeley National Laboratory, Berkeley, California 94720, United States;* Present Address: Linac Coherent Light Source, SLAC National Accelerator Laboratory, Menlo Park, California 94025, United States

**Philippe Wernet** − *Department of Physics and Astronomy, Uppsala University, 75120 Uppsala, Sweden;* orcid.org/0000-0001-7011-9072

**Alexander Föhlisch** − *Institut für Physik und Astronomie, Universität Potsdam, 14476 Potsdam, Germany; Institute for Methods and Instrumentation for Synchrotron Radiation Research, Helmholtz-Zentrum Berlin für Materialien und Energie, 12489 Berlin, Germany*

Complete contact information is available at: https://pubs.acs.org/10.1021/acs.jpclett.1c01401

## Notes

The authors declare no competing financial interest.

## ■ ACKNOWLEDGMENTS

R.M.J., S.E., and A.F. acknowledge funding from the ERC-ADG-2014 Advanced Investigator Grant No. 669531 EDAX under the Horizon 2020 EU Framework Program for Research and Innovation. N.H. and M.O. acknowledge funding by the Max Planck Society, the City of Hamburg and the collaborative research center SFB 925 of the German Science Foundation (DFG), project 170620586. S.E., M.H., W.Q., A.P., P.W., and A.F. acknowledge partial or full support by the Helmholtz-Virtual Institute VI419 "Dynamic Pathways in Multidimensional Landscapes". M.B. acknowledges funding from the Volkswagen foundation. This work was supported by the National Research Foundation of Korea (NRF) grants funded by the Korean Government (2016R1E1A1A01941978 and 2020R1A4A1017737). A.A.C., H.C., J.H.L., and R.W.S. acknowledge support through LBNL from the U.S. Department of Energy, Office of Science, Basic Energy Sciences, Chemical Sciences, Geosciences, and Biosciences Division under Contract No. DE-AC02-05-CH11231 within the Atomic, Molecular, and Optical Science program. This work, as well as the use of the Linac Coherent Light Source (LCLS) at SLAC National Accelerator Laboratory, is supported by the U.S. Department of Energy, Office of Science, Office of Basic Energy Sciences, under Contract No. DE-AC02-76SF00515, through the Materials Sciences and Engineering Division and the Scientific User Facilities Division, respectively. The SXR Instrument is funded by a consortium whose membership includes the LCLS, Stanford University through the Stanford Institute for Materials Energy Sciences (SIMES), Lawrence Berkeley National Laboratory (LBNL), University of Hamburg through the BMBF priority program FSP 301, and the Center for Free Electron Laser Science (CFEL).

## ■ REFERENCES

(1) Kalyanasundaram, K. Applications of Functionalized Transition Metal Complexes in Photonic and Optoelectronic Devices. *Coord. Chem. Rev.* **1998**, *177*, 347−414.

(2) Nazeeruddin, M. K.; Grätzel, M. Transition Metal Complexes for Photovoltaic and Light Emitting Applications. *Struct. Bonding (Berlin, Ger.)* **2007**, *123*, 113−175.

(3) Berardi, S.; Drouet, S.; Francàs, L.; Gimbert-Suriñach, C.; Guttentag, M.; Richmond, C.; Stoll, T.; Llobet, A. Molecular Artificial Photosynthesis. *Chem. Soc. Rev.* **2014**, *43*, 7501−7519.

(4) Ye, Z.; Zhang, R.; Song, B.; Dai, Z.; Jin, D.; Goldys, E. M.; Yuan, J. Development of a Functional Ruthenium(II) Complex for Probing Hypochlorous Acid in Living Cells. *Dalt. Trans.* **2014**, *43*, 8414.

(5) Wasylenko, D. J.; Ganesamoorthy, C.; Henderson, M. A.; Koivisto, B. D.; Osthoff, H. D.; Berlinguette, C. P. Electronic Modification of the $[Ru^{II}(tpy)(bpy)(OH_2)]^{2+}$ Scaffold: Effects on Catalytic Water Oxidation. *J. Am. Chem. Soc.* **2010**, *132*, 16094−16106.

(6) Dunn, A. R.; Dmochowski, I. J.; Bilwes, A. M.; Gray, H. B.; Crane, B. R. Probing the Open State of Cytochrome P450cam with Ruthenium-Linker Substrates. *Proc. Natl. Acad. Sci. U. S. A.* **2001**, *98*, 12420−12425.

(7) Siefermann, K. R.; Pemmaraju, C. D.; Neppl, S.; Shavorskiy, A.; Cordones, A. A.; Vura-Weis, J.; Slaughter, D. S.; Sturm, F. P.; Weise, F.; Bluhm, H.; et al. Atomic-Scale Perspective of Ultrafast Charge Transfer at a Dye-Semiconductor Interface. *J. Phys. Chem. Lett.* **2014**, *5*, 2753−2759.

(8) Van Kuiken, B. E.; Huse, N.; Cho, H.; Strader, M. L.; Lynch, M. S.; Schoenlein, R. W.; Khalil, M. Probing the Electronic Structure of a

Photoexcited Solar Cell Dye with Transient X-Ray Absorption Spectroscopy. *J. Phys. Chem. Lett.* **2012**, *3*, 1695−1700.
(9) Cole, J. M.; Gong, Y.; McCree-Grey, J.; Evans, P. J.; Holt, S. A. Modulation of N3 and N719 Dye···Tio 2 Interfacial Structures in Dye-Sensitized Solar Cells As Influenced by Dye Counter Ions, Dye Deprotonation Levels, And Sensitizing Solvent. *ACS Appl. Energy Mater.* **2018**, *1*, 2821−2831.
(10) Nazeeruddin, M. K.; Baranoff, E.; Grätzel, M. Dye-Sensitized Solar Cells: A Brief Overview. *Sol. Energy* **2011**, *85*, 1172−1178.
(11) Al-Afyouni, M. H.; Rohrabaugh, T. N.; Al-Afyouni, K. F.; Turro, C. New Ru(II) Photocages Operative with near-Ir Light: New Platform for Drug Delivery in the PDT Window. *Chem. Sci.* **2018**, *9*, 6711−6720.
(12) Cardin, C. J.; Kelly, J. M.; Quinn, S. J. Photochemically Active DNA-Intercalating Ruthenium and Related Complexes − Insights by Combining Crystallography and Transient Spectroscopy. *Chem. Sci.* **2017**, *8*, 4705−4723.
(13) Cordones, A. A.; Lee, J. H.; Hong, K.; Cho, H.; Garg, K.; Boggio-Pasqua, M.; Rack, J. J.; Huse, N.; Schoenlein, R. W.; Kim, T. K. Transient Metal-Centered States Mediate Isomerization of a Photochromic Ruthenium-Sulfoxide Complex. *Nat. Commun.* **2018**, *9*, 1989.
(14) Livshits, M. Y.; Wang, L.; Vittardi, S. B.; Ruetzel, S.; King, A.; Brixner, T.; Rack, J. J. An Excited State Dynamics Driven Reaction: Wavelength-Dependent Photoisomerization Quantum Yields in $[Ru(bpy)_2(dmso)_2]^{2+}$. *Chem. Sci.* **2020**, *11*, 5797−5807.
(15) Damrauer, N. H.; Cerullo, G.; Yeh, A.; Boussie, T. R.; Shank, C. V.; McCusker, J. K. Femtosecond Dynamics of Excited-State Evolution in $[Ru(bpy)_3]^{2+}$. *Science* **1997**, *275*, 54−57.
(16) Cannizzo, A.; Van Mourik, F.; Gawelda, W.; Zgrablic, G.; Bressler, C.; Chergui, M. Broadband Femtosecond Fluorescence Spectroscopy of $[Ru(bpy)_3]^{2+}$. *Angew. Chem., Int. Ed.* **2006**, *45*, 3174−3176.
(17) Auböck, G.; Chergui, M. Sub-50-Fs Photoinduced Spin Crossover in $[Fe(bpy)_3]^{2+}$. *Nat. Chem.* **2015**, *7*, 629−633.
(18) Malone, R. A.; Kelley, D. F. Interligand Electron Transfer and Transition State Dynamics in Ru(II)trisbipyridine. *J. Chem. Phys.* **1991**, *95*, 8970−8976.
(19) Wallin, S.; Davidsson, J.; Modin, J.; Hammarström, L. Femtosecond Transient Absorption Anisotropy Study on $[Ru(bpy)_3]^{2+}$ And $[Ru(bpy)(py)_4]^{2+}$: Ultrafast Interligand Randomization of the MLCT State. *J. Phys. Chem. A* **2005**, *109*, 4697−4704.
(20) Yeh, A. T.; Shank, C. V.; McCusker, J. K. Ultrafast Electron Localization Dynamics Following Photo-Induced Charge Transfer. *Science* **2000**, *289*, 935−938.
(21) Gawelda, W.; Pham, V. T.; Benfatto, M.; Zaushitsyn, Y.; Kaiser, M.; Grolimund, D.; Johnson, S. L.; Abela, R.; Hauser, A.; Bressler, C.; et al. Structural Determination of a Short-Lived Excited Iron(II) Complex by Picosecond X-Ray Absorption Spectroscopy. *Phys. Rev. Lett.* **2007**, *98*, 6−9.
(22) Gawelda, W.; Cannizzo, A.; Pham, V.; van Mourik, F.; Bressler, C.; Chergui, M. Ultrafast Nonadiabatic Dynamics of $[Fe^{II}(bpy)_3]^{2+}$ in Solution. *J. Am. Chem. Soc.* **2007**, *129*, 8199−8206.
(23) Lundberg, M.; Wernet, P. Resonant Inelastic X-Ray Scattering (RIXS) Studies in Chemistry: Present and Future. In *Synchrotron Light Sources and Free-Electron Lasers*; Springer International Publishing: Cham, Switzerland, 2019.
(24) Garg, K.; Engle, J. T.; Ziegler, C. J.; Rack, J. J. Tuning Excited State Isomerization Dynamics through Ground State Structural Changes in Analogous Ruthenium and Osmium Sulfoxide Complexes. *Chem. - Eur. J.* **2013**, *19*, 11686−11695.
(25) Gawelda, W.; Johnson, M.; De Groot, F. M. F.; Abela, R.; Bressler, C.; Chergui, M. Electronic and Molecular Structure of Photoexcited $[Ru^{II}(bpy)_3]^{2+}$ Probed by Picosecond X-Ray Absorption Spectroscopy. *J. Am. Chem. Soc.* **2006**, *128*, 5001−5009.
(26) Sato, T.; Nozawa, S.; Tomita, A.; Hoshino, M.; Koshihara, S.; Fujii, H.; Adachi, S. Coordination and Electronic Structure of Ruthenium(II)-Tris-2,2′-Bipyridine in the Triplet Metal-to-Ligand Charge-Transfer Excited State Observed by Picosecond Time-Resolved Ru K-Edge XAFS. *J. Phys. Chem. C* **2012**, *116*, 14232−14236.
(27) Ament, L. J. P.; Van Veenendaal, M.; Devereaux, T. P.; Hill, J. P.; Van Den Brink, J. Resonant Inelastic X-Ray Scattering Studies of Elementary Excitations. *Rev. Mod. Phys.* **2011**, *83*, 705−767.
(28) Jay, R. M.; Eckert, S.; Fondell, M.; Miedema, P. S.; Norell, J.; Pietzsch, A.; Quevedo, W.; Niskanen, J.; Kunnus, K.; Föhlisch, A. The Nature of Frontier Orbitals under Systematic Ligand Exchange in (Pseudo-)Octahedral Fe(II) Complexes. *Phys. Chem. Chem. Phys.* **2018**, *20*, 27745−27751.
(29) Kunnus, K.; Zhang, W.; Delcey, M. G.; Pinjari, R. V.; Miedema, P. S.; Schreck, S.; Quevedo, W.; Schröder, H.; Föhlisch, A.; Gaffney, K. J.; et al. Viewing the Valence Electronic Structure of Ferric and Ferrous Hexacyanide in Solution from the Fe and Cyanide Perspectives. *J. Phys. Chem. B* **2016**, *120*, 7182−7194.
(30) Temperton, R. H.; Skowron, S. T.; Handrup, K.; Gibson, A. J.; Nicolaou, A.; Jaouen, N.; Besley, E.; O'Shea, J. N. Resonant Inelastic X-Ray Scattering of a Ru Photosensitizer: Insights from Individual Ligands to the Electronic Structure of the Complete Molecule. *J. Chem. Phys.* **2019**, *151*, 074701.
(31) Hong, K.; Cho, H.; Schoenlein, R. W.; Kim, T. K.; Huse, N. Element-Specific Characterization of Transient Electronic Structure of Solvated Fe(II) Complexes with Time-Resolved Soft X-Ray Absorption Spectroscopy. *Acc. Chem. Res.* **2015**, *48*, 2957−2966.
(32) Van Kuiken, B. E.; Cho, H.; Hong, K.; Khalil, M.; Schoenlein, R. W.; Kim, T. K.; Huse, N. Time-Resolved X-Ray Spectroscopy in the Water Window: Elucidating Transient Valence Charge Distributions in an Aqueous Fe(II) Complex. *J. Phys. Chem. Lett.* **2016**, *7*, 465−470.
(33) Eckert, S.; Niskanen, J.; Jay, R. M.; Miedema, P. S.; Fondell, M.; Kennedy, B.; Quevedo, W.; Iannuzzi, M.; Föhlisch, A. Valence Orbitals and Local Bond Dynamics around N Atoms of Histidine under X-Ray Irradiation. *Phys. Chem. Chem. Phys.* **2017**, *19*, 32091−32098.
(34) Eckert, S.; Norell, J.; Miedema, P. S.; Beye, M.; Fondell, M.; Quevedo, W.; Kennedy, B.; Hantschmann, M.; Pietzsch, A.; Van Kuiken, B. E.; et al. Ultrafast Independent N−H and N−C Bond Deformation Investigated with Resonant Inelastic X-Ray Scattering. *Angew. Chem., Int. Ed.* **2017**, *56*, 6088−6092.
(35) Wernet, P.; Kunnus, K.; Josefsson, I.; Rajkovic, I.; Quevedo, W.; Beye, M.; Schreck, S.; Grübel, S.; Scholz, M.; Nordlund, D.; et al. Orbital-Specific Mapping of the Ligand Exchange Dynamics of $Fe(CO)_5$ in Solution. *Nature* **2015**, *520*, 78−81.
(36) Kunnus, K.; Josefsson, I.; Rajkovic, I.; Schreck, S.; Quevedo, W.; Beye, M.; Weniger, C.; Grübel, S.; Scholz, M.; Nordlund, D.; et al. Identification of the Dominant Photochemical Pathways and Mechanistic Insights to the Ultrafast Ligand Exchange of $Fe(CO)_5$ to $Fe(CO)_4EtOH$. *Struct. Dyn.* **2016**, *3*, 043204.
(37) Kunnus, K.; Josefsson, I.; Rajkovic, I.; Schreck, S.; Quevedo, W.; Beye, M.; Grübel, S.; Scholz, M.; Nordlund, D.; Zhang, W.; et al. Anti-Stokes Resonant X-Ray Raman Scattering for Atom Specific and Excited State Selective Dynamics. *New J. Phys.* **2016**, *18*, 1−9.
(38) Norell, J.; Jay, R. M.; Hantschmann, M.; Eckert, S.; Guo, M.; Gaffney, K. J.; Wernet, P.; Lundberg, M.; Föhlisch, A.; Odelius, M. Fingerprints of Electronic, Spin and Structural Dynamics from Resonant Inelastic Soft X-Ray Scattering in Transient Photo-Chemical Species. *Phys. Chem. Chem. Phys.* **2018**, *20*, 7243−7253.
(39) Jay, R. M.; Norell, J.; Eckert, S.; Hantschmann, M.; Beye, M.; Kennedy, B.; Quevedo, W.; Schlotter, W. F.; Dakovski, G. L.; Minitti, M. P.; et al. Disentangling Transient Charge Density and Metal-Ligand Covalency in Photoexcited Ferricyanide with Femtosecond Resonant Inelastic Soft X-Ray Scattering. *J. Phys. Chem. Lett.* **2018**, *9*, 3538−3543.
(40) Cordones, A. A.; Pemmaraju, C. D.; Lee, J. H.; Zegkinoglou, I.; Ragoussi, M.-E.; Himpsel, F. J.; de la Torre, G.; Schoenlein, R. W. Excited-State Charge Distribution of a Donor−$\pi$−Acceptor Zn Porphyrin Probed by N K-Edge Transient Absorption Spectroscopy. *J. Phys. Chem. Lett.* **2021**, *12*, 1182−1188.


https://doi.org/10.1021/acs.jpclett.1c01401
*J. Phys. Chem. Lett.* 2021, 12, 6676−6683

(41) Jay, R. M.; Eckert, S.; Mitzner, R.; Fondell, M.; Föhlisch, A. Quantitative Evaluation of Transient Valence Orbital Occupations in a 3d Transition Metal Complex as seen from the Metal and Ligand Perspective. *Chem. Phys. Lett.* **2020**, *754*, 137681.
(42) Jay, R. M.; Eckert, S.; Vaz da Cruz, V.; Fondell, M.; Mitzner, R.; Föhlisch, A. Covalency-Driven Preservation of Local Charge Densities in a Metal-to-Ligand Charge-Transfer Excited Iron Photosensitizer. *Angew. Chem., Int. Ed.* **2019**, *58*, 10742−10746.
(43) García-Lastra, J. M.; Cook, P. L.; Himpsel, F. J.; Rubio, A. Communication: Systematic Shifts of the Lowest Unoccupied Molecular Orbital Peak in X-Ray Absorption for a Series of 3d Metal Porphyrins. *J. Chem. Phys.* **2010**, *133*, 151103.
(44) Atkins, A. J.; González, L. Trajectory Surface-Hopping Dynamics Including Intersystem Crossing in $[Ru(bpy)_3]^{2+}$. *J. Phys. Chem. Lett.* **2017**, *8*, 3840−3845.
(45) Zhang, W.; Alonso-Mori, R.; Bergmann, U.; Bressler, C.; Chollet, M.; Galler, A.; Gawelda, W.; Hadt, R. G.; Hartsock, R. W.; Kroll, T.; et al. Tracking Excited-State Charge and Spin Dynamics in Iron Coordination Complexes. *Nature* **2014**, *509*, 345−348.
(46) Zhang, W.; Kjær, K. S.; Alonso-Mori, R.; Bergmann, U.; Chollet, M.; Fredin, L. A.; Hadt, R. G.; Hartsock, R. W.; Harlang, T.; Kroll, T.; et al. Manipulating Charge Transfer Excited State Relaxation and Spin Crossover in Iron Coordination Complexes with Ligand Substitution. *Chem. Sci.* **2017**, *8*, 515−523.
(47) Kjær, K. S.; Zhang, W.; Alonso-Mori, R.; Bergmann, U.; Chollet, M.; Hadt, R. G.; Hartsock, R. W.; Harlang, T.; Kroll, T.; Kubiček, K.; et al. Ligand Manipulation of Charge Transfer Excited State Relaxation and Spin Crossover in $[Fe(2,2'\text{-Bipyridine})_2(CN)_2]$. *Struct. Dyn.* **2017**, *4*, 044030.
(48) Kjær, K. S.; Kunnus, K.; Harlang, T. C. B.; Van Driel, T. B.; Ledbetter, K.; Hartsock, R. W.; Reinhard, M. E.; Koroidov, S.; Li, L.; Laursen, M. G.; et al. Solvent Control of Charge Transfer Excited State Relaxation Pathways in $[Fe(2,2'\text{-Bipyridine})(CN)_4]^{2-}$. *Phys. Chem. Chem. Phys.* **2018**, *20*, 4238−4249.



https://doi.org/10.1021/acs.jpclett.1c01401
*J. Phys. Chem. Lett.* 2021, 12, 6676−6683